Journal of
Materials Chemistry A

Accepted Manuscript

This article can be cited before page numbers have been issued, to do this please use: H. Fang, S. Sun, P. Liao, Y. Hu and J. Zhang, *J. Mater. Chem. A*, 2017, DOI: 10.1039/C7TA08985F.

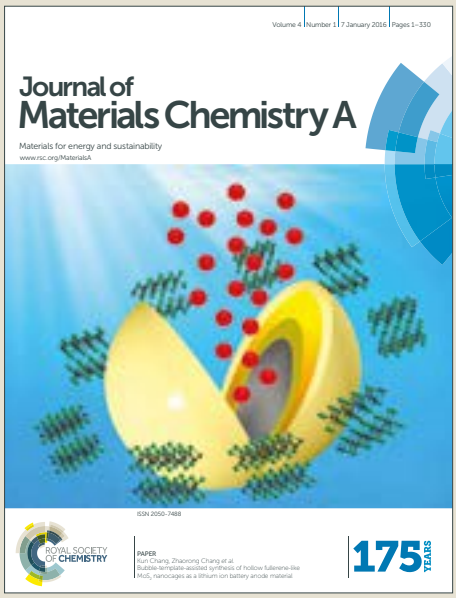

ROYAL SOCIETY OF CHEMISTRY

rsc.li/materials-a

ROYAL SOCIETY OF CHEMISTRY View Article Online
DOI: 10.1039/C7TA08985F

Journal Name

ARTICLE

Gold nanoparticles confined in imidazolium-based porous organic polymers to assemble a microfluidic reactor: Controllable growth and enhanced catalytic activity

Received 00th January 20xx,
Accepted 00th January 20xx

DOI: 10.1039/x0xx00000x

www.rsc.org/

Haobin Fang, Shujian Sun, Peisen Liao, Ya Hu* and Jianyong Zhang*

A synthetic strategy is developed to grow Au nanoparticles supported by imidazolium-based porous organic polymer (Au/IM-POP) along the inner surface of a fused-silica microfluidic capillary. The thickness of the hybrid Au/IM-POP material layers is tunable by changing the precursor concentration. A variety of imidazolium-based porous organic polymers are developed from tetrakis[4-(1-imidazolyl)phenyl]methane and bromo-functionalized linker molecules and fully characterized, which may be used to support Au nanoparticles. Additionally the IM-POPs and Au/IM-POPs show porosity and ability to uptake guest molecules. The capillary coated by Au/IM-POP is further assembled to obtain a catalytic microfluidic reactor. The catalytic activity of Au nanoparticles supported in the porous imidazolium polymer is probed by using the reduction of nitrobenzene derivatives flowing through the microfluidic reactor. The catalytic microfluidic reactor demonstrates significantly enhanced turnover frequency magnitudes in comparison with the corresponding reactions under batch conditions.

Introduction

The application of microfluidic reactors in organic synthesis has been explored extensively over recent years.[1-5] In microfluidic systems, reagent-containing fluid flows are confined in volumes that have micrometer-scale internal dimensions. This intrinsic confinement allows manipulation of the flow movement and fine control over the reaction conditions in a specific region. Additionally, the large surface area to volume ratio of microfluidic reactors offers increasing number of reaction sites exposed to reagents and rapid thermal transfer across the reactor.[6,7] Compared with bulk systems, chemical processes performed in microfluidic reactors possess many attractive advantages, such as low consumption of reagents,[8,9] precise selection of products,[3,10,11] improved energy efficiency[12] and applicability for explosive or toxic reactions.[13-15] As a versatile technological tool, microfluidics are a promising method to extend the utilization of supported catalysts from conventional flasks into continuous-flow synthesis.[16,17]

Supported metal nanoparticles on porous materials are a class of heterogeneous catalysts with potentially extremely high efficiency.[18-20] Among various porous materials, porous organic polymers (POPs) have attracted significant research interest for their high surface areas, well-defined pore structures and chemical stability.[21] When incorporating ionic building blocks into POPs, the organic frameworks exhibit enhanced electrostatic attraction with guest species carrying opposite charges.[22] Notable examples include imidazolium-based POPs (IM-POPs) for the *in situ* formation of Pd NPs reported by Wang and co-workers.[23] The resulting Pd NPs supported by the ionic POPs exhibit excellent catalytic property and show no obvious aggregation or leaching after mutiple runs. More recently, Dai and co-workers developed nanoporous ionic organic networks with an ionic density as high as three ion pairs per unit.[24] Au NPs supported by the ionic polymer frameworks show exceptionally good catalytic activity for the oxidation reaction of cyclohexanol to cyclohexanone. Most studies of POP-supported metal nanoparticles have been conducted in bulk state.[25,26] To improve the catalytic performance of these hybrid materials, research has focused on improvements on the optimization of the chemical composition and molecular arrangements.[27,28] However, no effort has been made to study the growth and catalytic property of the supported hybrid materials in microfluidic reactors.

In this study, we investigate the *in situ* growth and catalytic activity of Au NPs supported by IM-POPs on the inner surface of a microfluidic capillary. The insertion of imidazolium moieties has been demonstrated as an effective approach to creating cationic frameworks.[29-31] Through a finely designed surface functionalization process, the inner surface of the fused-silica capillary was coated with dangling bromo groups as anchors for the IM-POPs. Subsequent *in situ* growth of IM-POPs supported Au NPs along the surface was characterized

*Sun Yat-Sen University, MOE Laboratory of Polymeric Composite and Functional Materials, MOE Laboratory of Bioinorganic and Synthetic Chemistry, School of Materials Science and Engineering, Guangzhou 510275, China. *Email: huya3@mail.sysu.edu.cn; zhjyong@mail.sysu.edu.cn*

Electronic Supplementary Information (ESI) available: experimental details, characterization and sorption data of IM-POPs and Au/IM-POPs, and catalysis data. See DOI: 10.1039/x0xx00000x

using scanning electron microscopy (SEM) and transmission electron microscopy (TEM). Control over the thickness of the POPs layers could be achieved by facile adjustment of the precursor concentration. As a model system, nitroarene reduction was used to test the catalytic activity of Au NPs grown in the capillary.[32] The IM-POP-supported Au NPs constrained in the capillary exhibit excellent conversion and selectivity for the reduction of nitrobenzene derivatives into corresponding anilines. A significant increase in the TOF magnitude of the Au NPs grown in the capillary was measured presenting their enhanced catalytic efficiency.

Results and discussion

The synthetic scheme to grow Au NPs supported by IM-POP on the inner surface of a fused-silica capillary is presented in Figure 1. Prior to initiating the synthesis of IM-POP, the capillary surface undergoes a NaOH-induced hydroxylation process, and is then brominated by (3-bromopropyl)triethoxysilane treatment. Multiple bromination processes are required to ensure the homogeneity of bromo-functionalized coatings. Subsequently, reactants for the formation of POPs containing imidazolium cations are injected into the capillary using a syringe pump. The reactants include tetrakis[4-(1-imidazolyl)phenyl]methane (TIM) and 1,4-bis-bromomethyl-benzene (2BrB) (see below).[30] The imidazolium moieties of TIM can react with the bromo groups of 1,4-bis-bromomethyl-benzene to produce extended networks IM-POP-2BrB. Meanwhile, the coupling reaction of TIM with the dangling –Br groups on the surface leads to an improved connection between the IM-POPs and capillary. Due to the cationic nature of IM-POPs grown along the capillary surface, subsequently injected $AuCl_4^-$ anions are readily exchanged with Br^-. Following an *in situ* reduction induced by $NaBH_4$ solution, Au NPs are formed and stabilized within the porous channels of the IM-POP-2BrB layer.

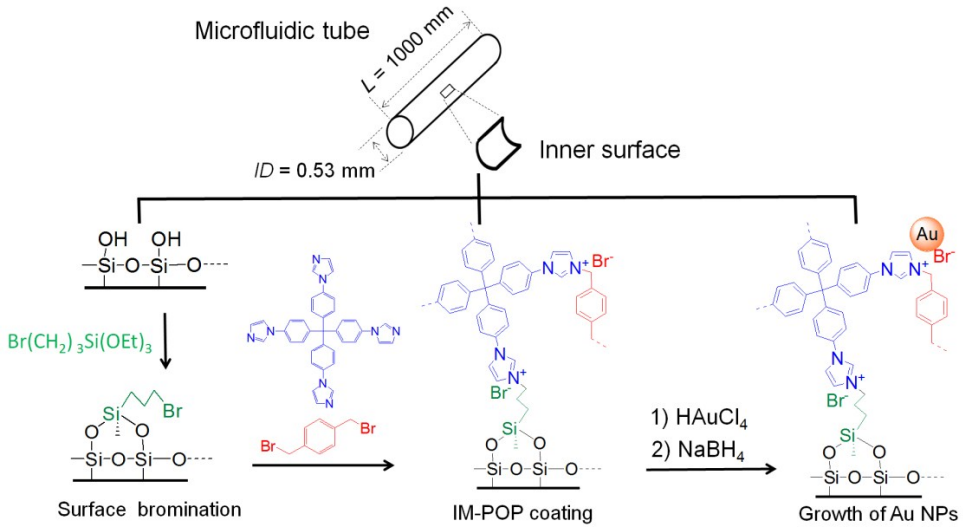

Fig. 1 Schematic illustration showing bromination and subsequent growth of IM-POP-supported Au NPs on the inner surface of a microfluidic capillary.

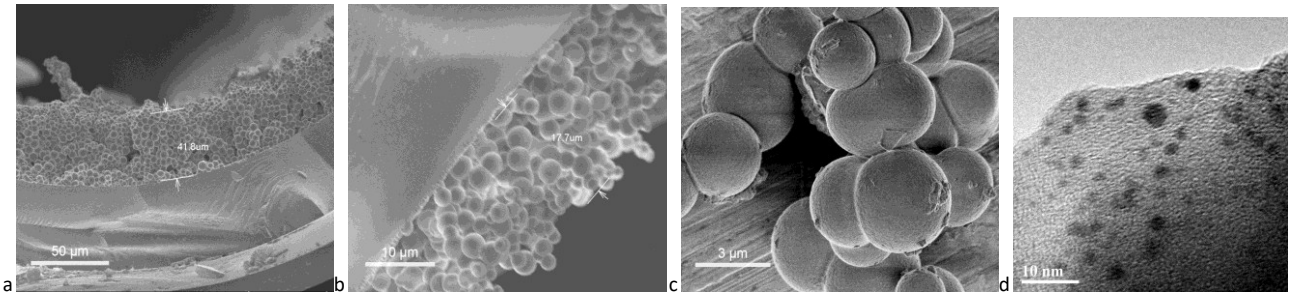

Fig. 2 Morphology studies of the IM-POP-2BrB-based Au NPs grown within the microfluidic capillary. a) SEM image of a thick Au/IM-POP-2BrB layer (Au/IM-POP-2BrB growth parameters: c_{TIM} = 0.046 mol L^{-1} and c_{2BrB} = 0.091 mol L^{-1} in $CHCl_3$ in a 1:1 volume ratio; injection speed 0.2 mL/min). b) SEM image of a thin Au/IM-POP-2BrB layer grown by diluting the $CHCl_3$ solutions of TIM and 2BrB by 5 times. c,d) SEM and high-resolution TEM images of Au/IM-POP-2BrB from the material presented in a).

The morphology of the resulting Au NPs supported by IM-POP-2BrB within the microfluidic capillary (denoted as c-Au/IM-POP-2BrB) is characterized using SEM and TEM (Figure 2). The SEM image of the capillary cross section confirms the growth of a homogeneous c-Au/IM-POP-2BrB layer with a thickness of 42.9 ± 5.8 μm (Figure 2a). The precursor concentration for the formation of IM-POP-2BrB, plays a key role in determining the thickness of the c-Au/IM-POP-2BrB layers. Figure 2b presents the SEM image of the cross section of a sample prepared by using a five-fold dilution of TIM and 2BrB dissolved in $CHCl_3$.

The thickness of the close-packed c-Au/IM-POP-2BrB layers is decreased to be 16.5 ± 2.9 µm due to this lowering concentration of reactants. SEM shows that c-Au/IM-POP-2BrB is macroscopically composed of interconnected polymer spheres with a diameter of 4.4 ± 0.9 µm (Figure 2c). This spherical particulate morphology is in agreement with those observed in other cationic POP systems.[24,33,34] The Au NPs supported by IM-POP-2BrB was characterized using high resolution TEM, and the TEM image determines nanoparticles of 3.8 ± 1.5 nm for c-Au/IM-POP-2BrB (Figure 2d).

To further understand the behaviours of Au/IM-POP in capillary, IM-POP and Au/IM-POP were prepared under batch conditions (denoted as b-IM-POP and b-Au/IM-POP, respectively) to measure the intrinsic properties of the materials. b-IM-POP-2BrB and b-Au/IM-POP-2BrB were prepared under batch conditions following the same POP synthesis and Au NPs growth procedures as presented in Figure 1 (see SI for experimental details). SEM measurements show that the b-Au/IM-POP-2BrB exhibit the same spherical morphology as compared with c-Au/IM-POP-2BrB (Figure S1). The sizes of the Au NPs supported by b-IM-POP are found to be closely correlated with the concentration of $HAuCl_4$/EtOH solutions used for Au NPs growth (Figure 3a,S2). The sizes of Au NPs decrease when increasing the concentrations of $HAuCl_4$ in the range of 0.0626 to 0.50 mmol L^{-1} (Figure 3b, Table S1). Further increase in the $HAuCl_4$ concentration ranging from 0.50 to 1.0 mmol L^{-1} results in increasing sizes of Au NPs. This concentration dependency can be explained by the two-step growth mechanism of Au NPs formation proposed by Polte and co-workers.[35] In the first step, the Au precursor, $AuCl_4^-$, is covered into metallic gold nuclei. Subsequently, Au NPs are formed from the nuclei via coalescence. At the high concentrations (0.50 to 1.0 mmol L^{-1}), a large number of nuclei exist and the coalescence is a size-determining step for the formation of Au NPs. Thus, an increasing concentration of $AuCl_4^-$ leads to a higher possibility for several adjacent nuclei to coalesce, and consequently an increasing NP size. In contrast, nucleation plays a decisive role in determining Au NP size at the low concentrations (0.0626 to 0.50 mmol L^{-1}). When increasing the concentration of $AuCl_4^-$ in this range, the number of nuclei is increased, thus the number of Au atoms in each of the nuclei is decreased.

The chemical structure of Au NPs grown within IM-POP-2BrB was probed using X-ray photoelectron spectroscopy (XPS). Figure 3c shows the Au 4f spectrum for b-Au/IM-POP-2BrB. The Au $4f_{7/2}$ core level was modeled with two components including two peaks at 83.5 and 85.0 eV corresponding to Au(0) and Au(I), respectively.[36-38] The small amount of Au(I) is suggested to be present on the surface of Au NPs and help stabilize them against electrostatic aggregation.[37,39] As shown in Figure 3d, PXRD patterns further prove the existence of crystalline Au NPs encapsulated in the IM-POP networks. For IM-POP-2BrB, the broad peak at around 22.5° indicates formation of an amorphous phase for IM-POP-2BrB.[30,40] After loading Au NPs, the amorphous nature of the host IM-POP matrix remains unchanged while the Au (111) lattice plane is detected as indicated by the strong peak at around 38.0°.[41,42]

The simultaneous presence of Br^- counterion is revealed by energy-dispersive X-ray (EDX) analysis (Figure S3). Cross-polarization magic-angle-spinning (CP/MAS) ^{13}C NMR supports the formation of imidazolium corresponding to the signal at 54.1 ppm (Figure S4). Fourier-transform infrared spectroscopy (FT-IR) of Au/IM-POP-2BrB and IM-POP-2BrB are nearly identical confirming the presence of organic imidazolium polymer backbone (Figure S5). Thermalgravimetric analysis (TGA) reveals that both IM-POP-2BrB and Au/IM-POP-2BrB are thermally stable at temperatures below 300 °C (Figure S6). At temperatures above 300 °C, the decompositions of the materials are activated.

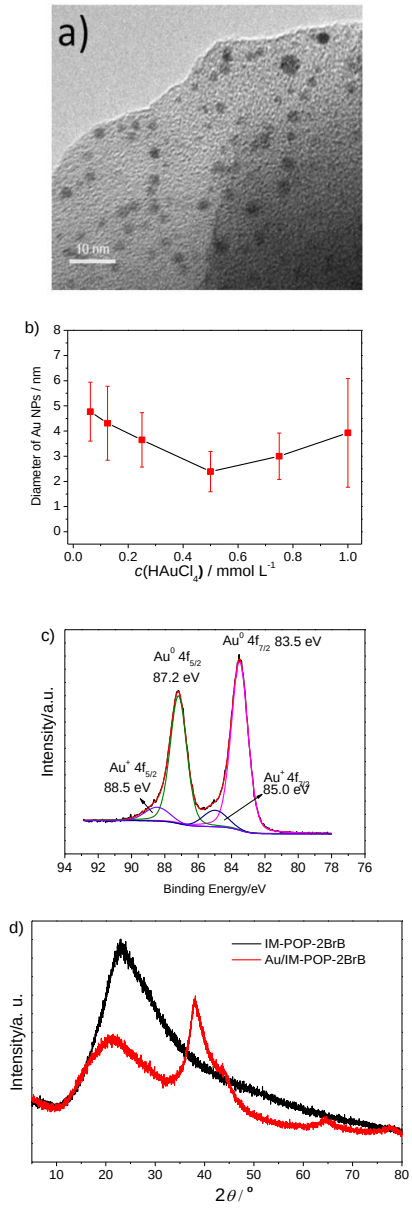

Fig. 3 Characterization of Au/IM-POP-2BrB synthesized under batch conditions, a) TEM image of Au/IM-POP-2BrB when using a $HAuCl_4$/EtOH solution at 0.5 mmol L^{-1}, b) diagram showing the sizes of Au NPs synthesized at various concentrations of $HAuCl_4$ (all the error bars in the inset represent standard deviations), c) XPS spectrum for Au/IM-POP-2BrB in the binding energy range of Au species, d) PXRD patterns of IM-POP-2BrB and Au/IM-POP-2BrB.

View Article Online
DOI: 10.1039/C7TA09255E

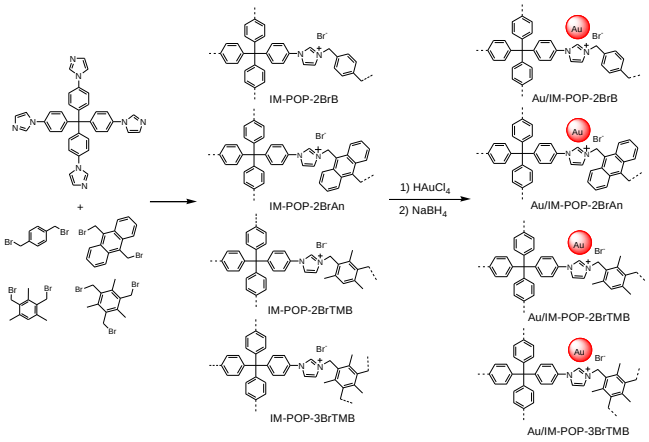

Scheme 1 Synthetic route to IM-POPs and Au/IM-POPs.

The synthesis of present imidazolium-based porous organic polymers can be extended from 1,4-bis-bromomethyl-benzene to a range of bromo-functionalized linker molecules by performing reactions with tetrakis[4-(1-imidazolyl)phenyl]methane under identical conditions (Scheme 1). These linker molecules include 9,10-bis(bromomethyl)anthracene (2BrAn), 2,4-bis-bromomethyl-1,3,5-trimethyl-benzene (2BrTMB) and 2,4,6-tris(bromomethyl)mesitylene (3BrTMB). Following the synthesis of IM-POPs, Au NPs were grown using $HAuCl_4$ solutions all at a concentration of 0.25 mmol L^{-1}. The resulting IM-POPs and Au/IM-POPs are characterized by various techniques including SEM, TEM, EDX, XPS, PXRD, CP/MAS NMR, FT-IR and TGA (See SI, Figure S1-S8 for synthesis and detailed characterization). As can be seen from the TEM images in Figure 4, spherical Au NPs are embedded within the matrix of IM-POPs formed by three linkers. The average sizes of Au NPs were measured to be 3.7 ± 0.8 nm, 4.2 ± 0.8 nm and 3.6 ± 0.9 nm for Au/IM-POP-2BrAn, Au/IM-POP-2BrTMB and Au/IM-POP-3BrTMB, respectively. These are similar to that measured from IM-POP-2BrB under similar conditions (3.7 ± 1.1 nm). It suggests that various imidazolium-based porous organic polymers may be used to support gold nanoparticles to assemble a microfluidic reactor. Since the Au NP sizes are not strongly correlated with the species of linker molecules, 1,4-bis-bromomethyl-benzene (2BrB) was chosen in the subsequent catalytic studies.

The porosity and sorption properties of IM-POPs and Au/IM-POPs were studied using gas and vapour sorption analysis. N_2 adsorption-desorption isotherms at 77 K demonstrate that IM-POP-2BrB has low adsorption capacity of 19.0 cm^2 g^{-1} with calculated Brunauer-Emmett-Teller (BET) surface area of 8.6 m^2 g^{-1} and total pore volume of 0.034 cm^3 g^{-1} (Figure S9). After loading Au NPs, the BET surface area and the total pore volume of Au/IM-POP-2BrB increases to 88.1 m^2 g^{-1} and 0.10 cm^3 g^{-1}, respectively. The low N_2 uptake of both the materials may be attributed to their flexible frameworks and charged pore channels which result in weak interaction between nitrogen and framework.[43] The slightly higher surface and pore volume of Au/IM-POP-2BrB may be attributed to the pillar effect of Au NPs to enlarge the pore channels. In contrast, MeOH sorption isotherms of both IM-POP-2BrB and Au/IM-POP-2BrB are type II, the uptake capacities of IM-POP-2BrB and Au/IM-POP-2BrB reach 351 cm^3 g^{-1} (50.1 wt%) and 234 cm^3 g^{-1} (33.4 wt%), respectively, at P/P_0 = 0.85 at 298 K (Figure S10). As compared to N_2, the remarkably increased MeOH uptake capacity is suggested to result from the higher temperature and the enhanced interaction between polar MeOH vapour and the charged network of IM-POP-2BrB and Au/IM-POP-2BrB.[44,45] Other IM-POP materials with various bromo-functionalized linker molecules show similar sorption behaviours. These results show that Au/IM-POPs have charged pore surfaces and are ready to capture guests.

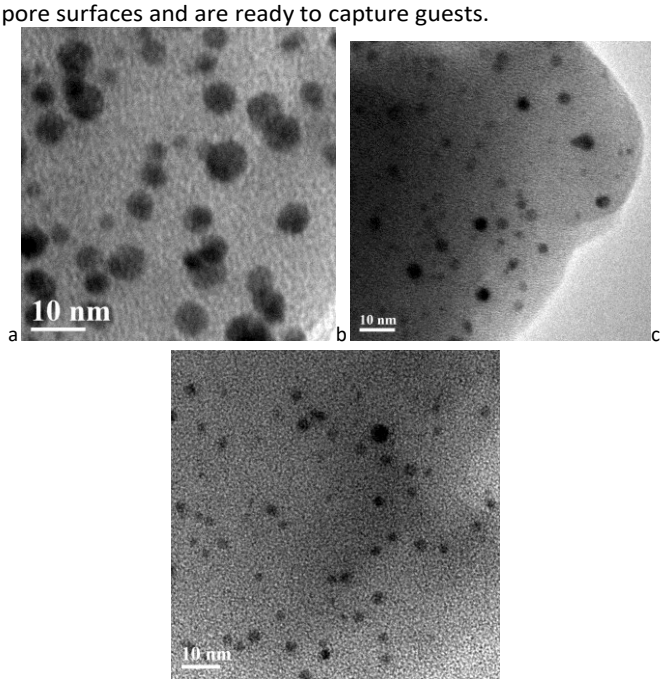

Fig. 4 TEM images showing the growth of Au NPs within IM-POPs synthesized with a range of bromo-functionalized linker molecules, (a) Au/IM-POP-2BrAn, (b) Au/IM-POP-2BrTMB and (c) Au/IM-POP-3BrTMB.

The catalytic performance of Au/IM-POP was evaluated as a representative in the reduction of nitroarene derivatives to corresponding anilines, which is an important transformation in organic chemistry and chemical industry, and also a model reaction to test the catalytic activity of Au NPs.[32,42,46,47] The reduction of 1-chloro-4-nitrobenzene to 4-chloroaniline was initially chosen as a probe reaction. The reaction was performed in both microfluidic reactors and flasks in order to compare the catalytic activity (see ESI for details and product characterization). Figure 5 shows the microfluidic reaction system containing the capillary functionalized with a layer of Au/IM-POP-2BrB material as heterogeneous catalyst. For a capillary with a length of 1.0 m, the reactant, 1-chloro-4-nitrobenzene (1 mmol), was dissolved in THF (4 mL). The reduction agent, $NaBH_4$ (3 mmol), was dissolved in water (2 mL). After mixing the solutions, 2 mL of the resulting mixture was taken to be introduced into the capillary using a syringe. The mixture (2 mL) passed through the capillary during 1.5 h controlled by the syringe pump. At room temperature, 1-chloro-4-nitrobenzene was catalytically reduced to product

View Article Online
DOI: 10.1039/C7TA08955F

that could be collected at the end of the capillary and tested using gas chromatography (GC). For measurements under batch conditions, Au/IM-POP-2BrB was added into the mixed reactants directly and the reaction was performed under Ar atmosphere.

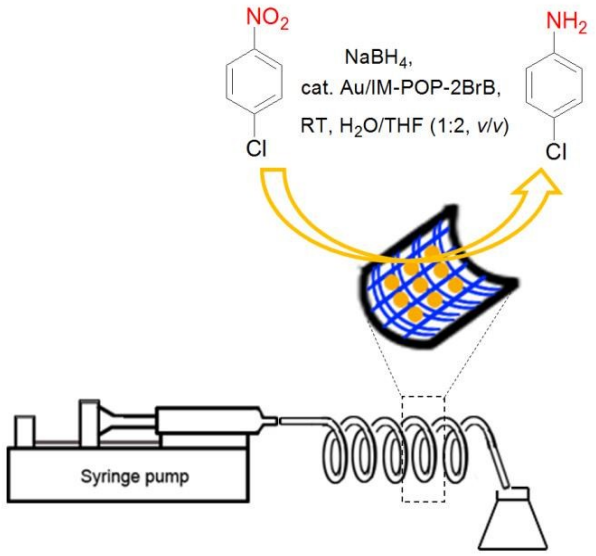

Fig. 5 Schematic representation of the microfluidic reactor assembled from an Au/IM-POP-functionalized capillary, and the reduction of nitrobenzene derivatives catalyzed by Au NPs on the inner capillary surface.

The catalytic reduction results are summarized in Table 1. Au/IM-POP-2BrB in the microfluidic reactor exhibits excellent catalytic performance for the reduction of 1-chloro-4-nitrobenzene into 4-chloroaniline in THF-H_2O (2:1, v/v). The effect of coating thickness was investigated, and c-Au/IM-POP with a coating thickness of 42.9 ± 5.8 μm shows more complete conversion (97%), and higher selectivity (98%) and TOF (6115 h^{-1}) when compared with those with thin coating (16.5 ± 2.9 μm with TOF 5827 h^{-1}) (Table 1, entry 1,6). The amount of Au in Au/IM-POP-2BrB was determined using either inductively coupled plasma (ICP) or atomic absorption spectroscopy (AAS) technique. The apparent turnover frequency (TOF) of the Au NPs supported by IM-POP was calculated as the amount of nitrobenzene that a mole of Au can concert per unit time.[48] In contrast, among b-Au/IM-POP prepared from various $HAuCl_4$ concentrations (0.25, 0.50 and 0.75 mmol L^{-1}), Au/IM-POP of 0.25 mmol L^{-1} shows higher conversion (98%), selectivity (> 99%) and TOF (647 h^{-1}) for the reduction of 1-chloro-4-nitrobenzene under batch conditions (Table 1, entry 7-9). The TOF values of b-Au/IM-POP-2BrB are measured to range from 607 h^{-1} to 647 h^{-1}. By confining Au/IM-POP hybrid materials within the capillary, a significant increase (up to 10 times) in the TOF of Au NPs is demonstrated. This improved TOF was possibly caused by the increasing proportion of Au NPs that could be exposed to the nitrobenzene derivatives when Au/IM-POP was transformed to the confined layer. This is suggested to result from the improved contact between substrate materials and the catalytic active sites of Au NPs by confining within the surface.[49]

Table 1 Reduction of nitrobenzene derivatives to anilines catalyzed by Au/IM-POP-2BrB at RT.

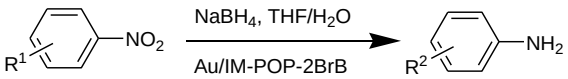

Entry	R	Catalyst[a]	Au content /mmol g^{-1}	*t*/h	Conv./%[b]	Sel./%[b]	TOF/h^{-1}
1[c]	$R^1 = R^2$ = 4-Cl	c-Au/IM-POP-2BrB thick	0.024	1.5	97	98	6115
2[d]				1.5	96	92	5724
3[e]				1.5	98	98	6037
4[f]				1.5	97	99	6037
5[g]				1.5	91	>99	5720
6[h]	$R^1 = R^2$ = 4-Cl	c-Au/IM-POP-2BrB thin	0.030	1.5	92	95	5827
7[i]	$R^1 = R^2$ = 4-Cl	b-Au/IM-POP-2BrB-1 (c_{HAuCl4} 0.25 mmol L^{-1})	0.062	3.0	98	>99	647
8[i]	$R^1 = R^2$ = 4-Cl	b-Au/IM-POP-2BrB-2 (c_{HAuCl4} 0.50 mmol L^{-1})	0.23	1.5	96	92	640
9[i]	$R^1 = R^2$ = 4-Cl	b-Au/IM-POP-2BrB-3 (c_{HAuCl4} 0.75 mmol L^{-1})	0.14	1.5	91	>99	607
10[c]	$R^1 = R^2$ = 4-H	c-Au/IM-POP-2BrB thick	0.024	1.5	99	99	6161
11[c]	$R^1 = R^2$ = 4-Me	c-Au/IM-POP-2BrB thick	0.024	1.5	98	97	5905
12[c]	$R^1 = R^2$ = 3-Me	c-Au/IM-POP-2BrB thick	0.024	1.5	92	95	5650
13[c]	$R^1 = R^2$ =2-Me	c-Au/IM-POP-2BrB thick	0.024	1.5	94	98	5841
14[c]	R^1 = 4-CHO, R^2 = 4-CH_2OH	c-Au/IM-POP-2BrB thick	0.024	1.5	92	94	5460

[a] c-Au/IM-POP-2BrB thick has a coating thickness of 42.9 ± 5.8 μm, and c-Au/IM-POP-2BrB thin has a coating thickness of 16.5 ± 2.9 μm. [b] Conv.: (conversion) and Sel. (selectivity) were determined by GC. [c] Conditions for c-Au/IM-POP-2BrB thick: capillary length, 1.0 m; injection speed, 3 μL min^{-1}; nitrobenzene derivatives, 0.33 mmol; $NaBH_4$, 1.0 mmol; Au/substrate, 0.01 mol%; THF-H_2O (2:1, *v*/*v*), 2.0 mL. [d-g] The first-fourth recycling runs of entry 1. [h] Conditions for c-Au/IM-POP-2BrB thin: capillary length, 2.0 m; injection speed, 3 μL min^{-1}; nitrobenzene derivatives, 0.15 mmol; $NaBH_4$, 0.45 mmol; Au/substrate, 0.01 mol%; THF-H_2O (2:1, *v*/*v*), 2.0 mL. [i] Conditions for b-Au/IM-POP-2BrB: nitrobenzene derivatives, 1.0 mmol; $NaBH_4$, 3.0 mmol; Au/substrate, 0.1 mol%; THF-H_2O (2:1, *v*/*v*), 6.0 mL.

The capillary of c-Au/IM-POP could be reused as shown in the reduction of 1-chloro-4-nitrobenzene. The catalytic activity of c-Au/IM-POP was maintained for over another four recycling runs (Table 1, entry 2-5). The Au content within the catalyst after four runs was experimentally measured to be 0.025 mmol g^{-1}, which is nearly identical to the value prior to initiating the reduction, showing the catalysis was heterogeneous.

The catalytic tests of c-Au/IM-POP were then extended to the reduction of a range of nitrobenzene derivatives. Nitrobenzene, 4-nitrotoluene, 3-nitrotoluene and 2-nitroluene were efficiently reduced into corresponding amines while 4-nitrobenzaldehyde was fully reduced into 4-aminobenzyl alcohol using the microfluidic reactor with thick Au/IM-POP-2BrB coating as catalyst (Table 1, entry 10-14). All the reactions catalyzed by c-Au/IM-POP-2BrB reach high conversion (≥ 92 %), selectivity (≥ 94 %) and TOF (≥ 5460 h^{-1}) after 1.5 h. By comparison, the steric hindrance or electron-withdrawing groups on the benzene rings have no obvious effect on the catalytic activity of c-Au/IM-POP-2BrB.[42]

Conclusions

In summary, we have successfully developed a strategy for fabricating a catalytic microfluidic reactor via coating Au/IM-POP hybrid materials along the inner surface of a microfluidic capillary. A variety of imidazolium-based porous organic polymers are prepared from nucleophilic substitution reactions between tetrakis[4-(1-imidazolyl)phenyl]methane and bromo-functionalized linker molecules, e.g., 1,4-bis-bromomethyl-benzene (2BrB), which and fully characterized and may be used to support Au nanoparticles. The diameter sizes of Au NPs gown within the IM-POP depend strongly on the concentration of $HAuCl_4$ solutions. The IM-POPs and Au/IM-POPs show porosity and ability to uptake guest molecules. The thickness of the Au/IM-POP coating on the capillary is tuneable by changing the precursor concentration. The capillary is further assembled into a microfluidic reactor for the reduction of nitrobenzene derivatives into corresponding anilines catalyzed by the IM-POP-supported Au NPs. The microfluidic reactor with the Au/IM-POP-2BrB coating exhibits significantly higher catalytic efficiency in terms of TOF than the corresponding catalyst under batch conditions (6161 vs 647 h^{-1}). These results demonstrate the significance of improving the current catalytic activity of supported noble metal catalysts by a combination with microfluidic technology. The thickness controllable growth of the Au/IM-POP in the capillary provides flexible amount of catalysts that can be chosen. The significantly enhanced TOF exhibited by the Au/IM-POP suggests the capillary confinement plays a crucial role in increasing the efficiency of each catalytic site and reducing the amount of noble metal catalysts.

Conflicts of interest

There are no conflicts to declare.

Acknowledgements

View Article Online
DOI: 10.1039/C7TA08985F

We gratefully acknowledge the NSFC (51573216), the NSF of Guangdong Province (S2013030013474) and the FRF for the Central Universities (16lgjc66, 17lgpy03) for financial support.

Notes and references

1 K. S. Elvira, X. C. i Solvas, R. C. R. Wootton and A. J. deMello, *Nat. Chem.*, 2013, **5**,905-915.
2 T. Rodrigues, P. Schneider and G. Schneider, *Angew. Chem., Int. Ed.*, 2014, **53**, 5750-5758.
3 H. Kim, K.-I. Min, K. Inoue, D. J. Im, D.-P. Kim and J.-i. Yoshida, *Science*, 2016, **352**, 691-694.
4 H. P. L. Gemoets, Y. Su, M. Shang, V. Hessel, R. Luque and T. Noel, *Chem. Soc. Rev.*, 2016, **45**, 83-117.
5 P. W. Miller, L. E. Jennings, A. J. deMello, A. D. Gee, N. J. Long and R. Vilar, *Adv. Synth. Catal.*, 2009, **351**, 3260-3268.
6 H. Lindstrom, R. Wootton and A. Iles, *AICHE J.*, 2007, **53**, 695-702.
7 J. Zhang, C. Gong, X. Zeng and J. Xie, *Coord. Chem. Rev.*, 2016, **324**, 39-53.
8 J. R. Goodell, J. P. McMullen, N. Zaborenko, J. R. Maloney, C.-X. Ho, K. F. Jensen, J. A. Porco Jr and A. B. Beeler, *J. Org. Chem.*, 2009, **74**, 6169-6180.
9 R. L. Hartman, J. P. McMullen and K. F. Jensen, *Angew. Chem. Int. Ed.*, 2011, **50**, 7502-7519.
10 T. Asai, A. Takata, Y. Ushiogi, Y. Iinuma, A. Nagaka and J.-i. Yoshida, *Chem. Lett.*, 2011, **40**, 393-395.
11 A. Nagaki, K. Imai, S. Ishiuchi and J.-i Yoshisa, *Angew. Chem. Int. Ed.*, 2015, **54**, 1914-1918.
12 B. Pieber and C. O. Kappe, *Green Chem.*, 2013, **15**, 320-324.
13 C.-C. Lee, G. Sui, A. Elizarov, C. J. Shu, Y.-S. Shin, A. N. Dooley, J. Huang, A. Daridon, P. Wyatt and D. Stout, *Science*, 2005, **310**, 1793-1796.
14 C. Audubert, O. J. G. Marin and H. Lebel, *Angew. Chem. Int. Ed.*, 2017, **56,** 6294-6297.
15 B. Picard, B. Gouilleux, T. Lebleu, J. Maddaluno, I. Chataigner, M. Penhoat, F.-X. Felpin, P. Giraudeau and Julien Legros, *Angew. Chem. Int. Ed.*, 2017, **56,** 7568-7572.
16 H. Liu, J. Feng, J. Zhang, P. W. Miller, L. Chen and C.-Y. Su, *Chem. Sci.*, 2015, **6**, 2292-2296.
17 R. Munirathinam, J. Huskens and W. Verboom, *Adv. Synth. Catal.*, 2015, **357**, 1093-1123.
18 R. J. White, R. Luque, V. L. Budarin, J. H. Clark and D. J. Macquarrie, *Chem. Soc. Rev.*, 2009, **38**, 481-494.
19 C. R. Kim, T. Uemura and S. Kitagawa, *Chem. Soc. Rev.*, 2016, **45**, 3828-3845.
20 Q. Yang, Q. Xu and H.-L. Jiang, *Chem. Soc. Rev.*, 2017, **46**, 4774-4808.
21 Y. Zhang and S. N. Riduan, *Chem. Soc. Rev.*, 2012, **41**, 2083-2094.
22 J.-K. Sun, M. Antonietti and J. Yuan, *Chem. Soc. Rev.*, 2016, **45**, 6627-6656.
23 H. Zhao, Y. Wang and R. Wang, *Chem. Commun.*, 2014, **50**, 10871-10874.
24 P. Zhang, Z.-A. Qiao, X. Jiang, G. M. Veith and S. Dai, *Nano Lett.*, 2015, **15**, 823-828.
25 A. Modak, M. Pramanik, S. Inagaki and A. Bhaumik, *J. Mater. Chem. A*, 2014, **2**, 11642-11650.
26 X. Gu, Z.-H. Lu, H.-L. Jiang, T. Akita and Q. Xu, *J. Am. Chem. Soc.*, 2011, **133**, 11822-11825.
27 P. Kaur, J. T. Hupp and S. T. Nguyen, *ACS Catal.*, 2011, **1**, 819-835.
28 X. Zou, H. Ren and G. Zhu, *Chem. Commun.*, 2013, **49**, 3925-3936.

View Article Online
DOI: 10.1039/C7TA08985F

29 Y. Su, Y. Wang, X. Li, X. Li and R. Wang, *ACS Appl. Mater. Interfaces*, 2016, **8**, 18904-18911.
30 M. Lin, S. Wang, J. Zhang, W. Luo, H. Liu, W. Wang and C.-Y. Su, *J. Mol. Catal. A Chem.*, 2014, **394**, 33-39.
31 K. Park, K. Lee, H. Kim, V. Ganesan, K. Cho, S. K. Jeong and S. Yoon, *J. Mater. Chem. A*, 2017, **5**, 8576-8582.
32 T. Aditya, A. Pal and T. Pal, *Chem. Commun.*, 2015, **51**, 9410-9431.
33 Q. Zhang, S. Zhang and S. Li, *Macromolecules*, 2012, **45**, 2981-2988.
34 A. K. Chaudhari, I. Han and J. C. Tan, *Adv. Mater.*, 2015, **27**, 4438-4446.
35 J. Polte, R. Erler, A. F. Thünemann, S. Sokolov, T. T. Ahner, K. Rademann, F. Emmerling and R. Kraehnert, *ACS Nano*, 2010, **4**, 1076-1082.
36 J. Xie, Y. Zheng and J. Y. Ying, *J. Am. Chem. Soc.*, 2009, **131**, 888-889.
37 S. S. Shankar, A. Rai, A. Ahmad and M. Sastry, *Chem. Mater.*, 2005, **17**, 566-572.
38 Z. Dong, X. Le, Y. Liu, C. Dong and J. Ma, *J. Mater. Chem. A*, 2014, **2**, 18775-18785.
39 Y.-C. Liu and T. C. Chuang, *J. Phys. Chem. B*, 2003, **107**, 12383-12386.
40 A. Modak, M. Nandi, J. Mondal and A. Bhaumik, *Chem. Commun.*, 2012, **48**, 248-250.
41 X.-Y. Hu, T. Xiao, C. Lin, F. Huang and L. Wang, *Acc. Chem. Res.*, 2014, **47**, 2041-2051.
42 Y. Su, X. Li, Y. Wang, H. Zhong and R. Wang, *Dalton Trans.*, 2016, **45**, 16896-16903.
43 S. Wang, Q. Yang, J. Zhang, X. Zhang, C. Zhao, C.-Y. Su, *Inorg. Chem.*, 2013, **52**, 4198-4204.
44 S. Bourrelly, B. Moulin, A. Rivera, G. Maurin, S. Devautour-Vinot, C. Serre, T. Devic, P. Horcajada, A. Vimont, G. Clet, M. Daturi, J.-C. Lavalley, S. Loera-Serna, R. Denoyel, P. L. Llewellyn and G. Férey, *J. Am. Chem. Soc.*, 2010, **132**, 9488-9498.
45 K. Nakagawa, D. Tanaka, S. Horike, S. Shimomura, M. Higuchi and S. Kitagawa, *Chem. Commun.*, 2010, **46**, 4258-4260.
46 L. He, L.-C. Wang, H. Sun, J. Ni, Y. Cao, H.-Y. He and K.-N. Fan, *Angew. Chem., Int. Ed.*, 2009, **48**, 9538-9541.
47 S. Menuel, B. Leger, A. Addad, E. Monflier and F. Hapiot, *Green Chem.*, 2016, **18**, 5500-5509.
48 A. N. Oldacre, A. E. Friedman and T. R. Cook, *J. Am. Chem. Soc.*, 2017, **139**, 1424-1427.
49 L. Luza, C. P. Rambor, A. Gual, J. Alves Fernandes, D. Eberhardt and J. Dupont, *ACS Catal.*, 2017, **7**, 2791-2799.

View Article Online
DOI: 10.1039/C7TA08985F

Table of Contents

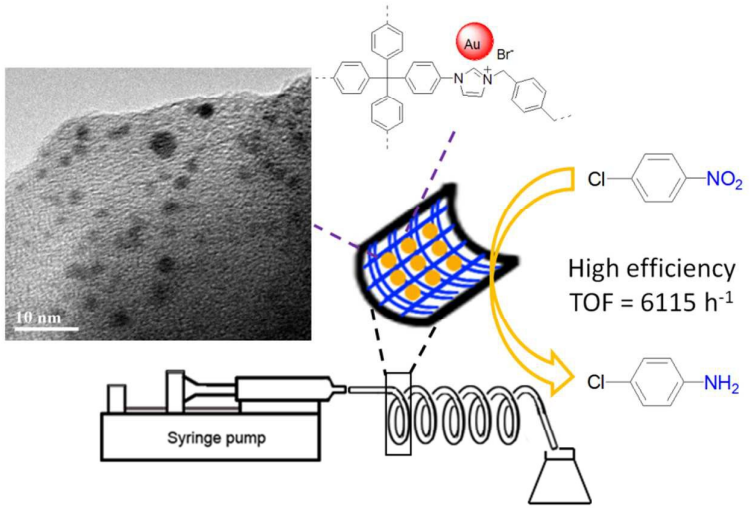

Gold nanoparticles confined in imidazolium-based porous organic polymers show high activity in a microfluidic reactor.